Journal of Zhejiang University SCIENCE A
ISSN 1673-565X (Print); ISSN 1862-1775 (Online)
www.zju.edu.cn/jzus; www.springerlink.com
E-mail: jzus@zju.edu.cn

Simulation of turbulent combustion in DLR Scramjet*

ZOU Jian-feng†, ZHENG Yao, LIU Ou-zi†‡
(*School of Aeronautics and Astronautics, Zhejiang University, Hangzhou 310027, China*)
†E-mail: zoujianfeng@zju.edu.cn; liuouzi@hotmail.com
Received Feb. 10, 2007; revision accepted Apr. 17, 2007

Abstract: Turbulent combustion in a DLR (German Aerospace Center) Scramjet engine was simulated using the newly-proposed Partially Resolved Numerical Simulation (PRNS) procedure. The PRNS procedure uses temporal filtering to define large-scale turbulence, and the model developed to account for unresolved scales is grid independent. No problem about inner commutation error and inconsistencies will arise from the PRNS, while such issues are of concern in traditional Large Eddy Simulation (LES) methods. The mean results have good agreement with the experiment data and the flow structures with small scales are well resolved.

Key words: Scramjet, Turbulent combustion, Unstructured grid, Finite volume method
doi:10.1631/jzus.2007.A1053 **Document code:** A **CLC number:** O35

INTRODUCTION

An increasing research effort has been made to investigate high speed turbulent combustion numerically, which is resulted from the interests in hypersonic air breathing propulsion.

A serious issue about turbulent combustion is the simulation of turbulence with multi-scale feature. For the traditional Large Eddy Simulation (LES) or hybrid RANS/LES approaches (Spalart *et al*., 1997; Bush and Mani, 2001; Fan *et al*., 2001; Georgiadis *et al*., 2001; Menter *et al*., 2003; Nichols and Nelson, 2001; Strelets, 2001), spatially filtered equations are used to compute the resolved scales of turbulence and certain sub-grid models for unresolved scales. There are several drawbacks associated with the spatially filtered equations and sub-grid models, which are stated by Shih and Liu (2004; 2005), i.e. the inconsistency between the filter function and sub-grid models, the commutation error due to the non-uniform computational mesh, the grid-dependent solu-

‡ Corresponding author
* Project supported by the National Natural Science Foundation of China (No. 90405003), and the China Postdoctoral Science Foundation (No. 20060390339)

grid-dependent solution, and the effect of numerical dissipation introduced by higher- order schemes.

Shih and Liu (2004; 2005) proposed a new methodology of Partially Resolved Numerical Simulation (PRNS) based on temporal filtering and demonstrated that, with the so-called "resolution control parameter", one can carry out a unified simulation from RANS towards LES or vise versa. This methodology does not involve spatial filtering, and there will be no issues about commutation errors, inconsistencies between the filter and sub-grid scale models, etc.

Shih and Liu (2004; 2005) have computed the turbulent flow for pipe flow and LM6000 combustor with the preliminary results being encouraging. Cai and Ladeinde (2006) provided their evaluation on the PRNS procedure for near-wall turbulence prediction.

In the present study, the PRNS will be coupled with our own combustion code, which is expected to present a more encouraging and accurate description for turbulence in the Scramjet engine.

The turbulence in the DLR Scramjet engine is investigated with our combustion code. The available numerical and experimental data for DLR Scramjet engine was presented by Oevermann (2000) and used for benchmark. Our work will focus on

accurate simulation of turbulence in Scramjet combustion engines.

MATHEMATIC FORMULATION AND NUMERICAL METHOD

Governing equations

The equations representing reacting flows are the 3D and unsteady forms of the compressible Navier-Stokes equations and the species continuity equations. These equations are written as

$$\frac{\partial \boldsymbol{Q}}{\partial t}+\nabla \boldsymbol{F}=\boldsymbol{H}, \tag{1}$$

where $\boldsymbol{Q}$ is the vector of the conservative variables

$$\boldsymbol{Q}=(\rho,\rho u,\rho v,\rho E,\rho Y_i)^{\mathrm{T}}, \tag{2}$$

with ρ being the density, u, v the velocity components and E the energy per unit mass, respectively.

The flux tensor $\boldsymbol{F}$=($\boldsymbol{f}$, $\boldsymbol{g}$) is split into the inviscid part and viscous part. The inviscid part has the following form

$$\boldsymbol{f}_{\mathrm{inv}}=\begin{pmatrix}\rho u\\ \rho u^2+P\\ \rho uv\\ (\rho E+P)u\\ \rho uY_i\end{pmatrix},\quad \boldsymbol{g}_{\mathrm{inv}}=\begin{pmatrix}\rho v\\ \rho uv\\ \rho v^2+P\\ (\rho E+P)v\\ \rho vY_i\end{pmatrix}. \tag{3}$$

The viscous part becomes

$$\boldsymbol{f}_{\mathrm{vis}}=\begin{pmatrix}0\\ -\tau_{xx}\\ -\tau_{xy}\\ -(u\tau_{xx}+v\tau_{xy})+q_x\\ q_{i,x}\end{pmatrix},\ \boldsymbol{g}_{\mathrm{vis}}=\begin{pmatrix}0\\ -\tau_{xy}\\ -\tau_{yy}\\ -(u\tau_{xy}+v\tau_{yy})+q_y\\ q_{i,y}\end{pmatrix}. \tag{4}$$

The stress tensor is given by Eq.(5):

$$\tau_{xx}=\frac{2}{3}\mu\left(2\frac{\partial u}{\partial x}-\frac{\partial v}{\partial y}\right),\quad \tau_{xy}=\mu\left(2\frac{\partial u}{\partial y}+\frac{\partial v}{\partial x}\right),$$

$$\tau_{yy}=\frac{2}{3}\mu\left(2\frac{\partial v}{\partial y}-\frac{\partial u}{\partial x}\right), \tag{5}$$

where μ is the shear viscosity that can be achieved with Sutherland's Law.

The heat flux terms q_x and q_y are given by Fourier's Law. The thermal conductivity coefficient, the shear viscosity and the diffusive coefficient are associated by the Prandtl number and the Schmidt number.

The source terms on the right hand side of Eq.(1) can be written as

$$\boldsymbol{H}=(0,0,0,\dot{\omega}_T,\dot{\omega}_i), \tag{6}$$

where $\dot{\omega}_T$ is the rate of heat release and $\dot{\omega}_i$ the reaction rate of species i, which can be computed by finite rate chemistry.

Partially resolved numerical simulation

Turbulence contains a wide spectrum of scales, ranging from the Kolmogorov small scale to the entire domain of the flow field. Shih and Liu (2004)'s PRNS uses temporally filtered governing equations to describe the resolved large scales of turbulence.

In our code, the tophat filter with ΔT is used to filter the governing equations. The large scale variable is calculated as

$$\bar{\phi}(t,x_i)=\frac{1}{\Delta T}\int_{t-\Delta T/2}^{t+\Delta T/2}\phi(t',x_i)\mathrm{d}t',\quad \tilde{\phi}=\frac{\overline{\rho\phi}}{\bar{\rho}}. \tag{7}$$

With the temporal filter given in Eq.(7), the governing equations for the resolved turbulences can be written as

$$\begin{cases}\bar{\rho}_{,t}+(\bar{\rho}\tilde{u}_i)_{,i}=0,\\ (\bar{\rho}\tilde{u}_i)_{,t}+(\bar{\rho}\tilde{u}_i\tilde{u}_j)_{,j}=-\bar{P}_{,i}-\tau^*_{ij,j}\\ \qquad\qquad +(2\bar{\mu}\tilde{S}_{ij}-2\delta_{ij}\bar{\mu}\tilde{S}_{kk}/3)_{,j},\\ (\bar{\rho}\tilde{E})_{,t}+(\bar{\rho}\tilde{u}_i\tilde{E})_{,i}=(\bar{\kappa}\tilde{T})_{,i}+\overline{PS}_{kk}-q^*_{i,i}\\ \qquad\qquad +(2\bar{\mu}\tilde{S}_{ij}\tilde{S}_{ij}-2\bar{\mu}\tilde{S}_{kk}\tilde{S}_{ii}/3)+\bar{\omega}_T,\\ (\bar{\rho}\tilde{Y}_m)_{,t}+(\bar{\rho}\tilde{u}_i\tilde{Y}_m)_{,i}=-q^*_{mi,i}+(\bar{\rho}\overline{D}_m\tilde{Y}_{m,i})_{,i}+\bar{\omega}_m,\end{cases} \tag{8}$$

where $S_{ij}=(u_{i,j}+u_{j,i})/2$, $\tau^*_{ij}=\bar{\rho}(\tilde{u}_i\tilde{u}_j-\tilde{u}_i\tilde{u}_j)$,

$q_i^* = \overline{\rho}(\tilde{u}_i\tilde{E} - \tilde{u}_i\tilde{E})$, $q_{mi}^* = \overline{\rho}(\tilde{u}_i\tilde{Y}_m - \tilde{u}_i\tilde{Y}_m)$. τ_{ij}^*, q_i^* and q_{mi}^* represent the unresolved small turbulence scales in the filtered equations. These unresolved stress and fluxes should be modelled appropriately. Since the temporal filter based on ΔT is used and the unresolved terms have nothing to do with the grid width, the small scale model should be grid independent as well.

In our code, the unresolved terms are written as the following algebraic expressions by the eddy viscosity assumption (only the stress term is given):

$$\tau_{ij}^* = -2\mu_t(\tilde{S}_{ij} - \tilde{\delta}_{ij}\tilde{S}_{kk}/3) + 2\delta_{ij}\kappa/3. \quad (9)$$

Here a two-equation κ-ε model is developed to calculate the eddy viscosity:

$$\mu_t = R_{\mathrm{cp}}(\Delta T)C_\mu\overline{\rho}\kappa^2/\varepsilon, \quad (10)$$

where C_μ is a model coefficient, κ is the unresolved turbulent kinetic energy and ε is the unresolved dissipation rate. The value of parameter C_μ and the detailed transport equations of κ and ε can be found in (Shih and Liu, 2004).

The most interesting parameter R_{cp}, which is a function of temporal width, is called "resolution control parameter". In the traditional LES simulation, the low end of the resolved turbulence scales is determined by the grid spacing and the sub-grid model used to model the unresolved scale is grid dependent. Therefore, a fine grid is needed to obtain an accurate result. Otherwise, the sub-grid model with a coarse grid will give an incorrect evaluation of the unresolved scales. It is not the case for the PRNS simulation. In PRNS, the low end of the resolved scales is limited by the temporal width. The model of the unresolved scales is independent of the grid width and uses R_{cp} to evaluate the effect of the temporal filter. Thus the PRNS can produce reasonable results on a coarse grid as well as a fine grid. And by changing the parameter R_{cp} from 0 to 1, the PRNS will act as DNS or RANS. With this feature, we can always obtain physical solution to complex turbulent flows, according to the turbulence scales needed to resolve and the current computer capability. The validation and some applications of PRNS can be found in (Shih and Liu, 2004; Cai and Ladeinde, 2006).

Numerical methods

The governing equations are solved by the finite volume method based on an unstructured grid. The cell-vertex space discretization is used. In order to obtain an accurate solution, third order finite-element type Taylor-Galerkin scheme and multi-stage Runge-Kutta temporal integration are developed. The artificial viscosity model is provided to model smooth shock waves. The characteristic-based condition is used to handle the waves into or out of the computational boundaries.

DLR SCRAMJET ENGINE

Geometry model

Fig.1 presents a geometry model of the DLR Scramjet engine. The total length in the streamwise direction is 300 mm. The hydrogen is injected from the tail of the strut structure, which has a delta shape with an angle of 12°. The top boundary of the combustor has an angle of 3° with the horizontal line.

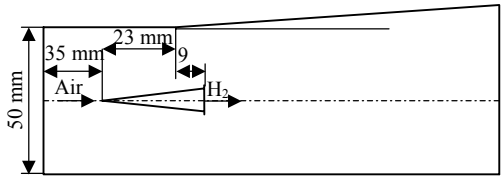

Fig.1 Geometry of the DLR Scramjet engine

Grid generation

The computational domain is divided into 97570 triangular elements and 49744 nodes. The computational points are stretched in the vicinity of boundaries, i.e. the delta strut, the inlet, the outlet, the top and the bottom walls (Fig.2). The grid size near the delta strut is about 0.25 mm. The wake flow near the center line is the main mixing region, and fine elements should be placed to obtain a good description of the turbulent mixing. Hence, grid stretching is also conducted in the wake region.

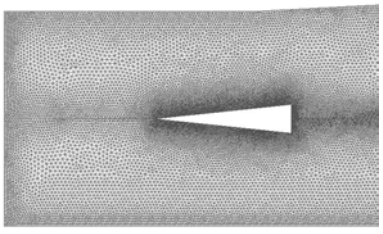

Fig.2 Computational grid near the delta-shape strut

Boundary conditions

The air and fuel inlets are supersonic conditions, which should be specified with all variables as given in Table 1. Neumann boundary conditions are used for all variables at outlet. At fixed walls and the struts, the slip conditions are applied. Hence, in our present study, the exact physical flows near boundary layers are not computed in detail.

Table 1 Variable values for air and hydrogen inlets

Variables	Air	H_2
Ma	2.0	1.0
u (m/s)	730	1200
T (K)	340	250
P (Pa)	101325	101325
ρ (kg/m^3)	1.002	0.097
Y_{O_2}	0.232	0
Y_{N_2}	0.736	0
Y_{H_2O}	0.032	0
Y_{H_2}	0	1

RESULTS AND DISCUSSIONS

In the present study, the code with PRNS for solving turbulent reactions is used to investigate the supersonic combustion in the DLR Scramjet engine. The simulation involves the third order finite-element type scheme and Runge-Kutta temporal integration. The value of parameter R_{cp} required by PRNS is 0.38. The PRNS with R_{cp}=0.38 is proposed by Shih and Liu (2005), which will lead to LES type PRNS solutions over a wide range of Reynolds numbers.

All computational tasks are performed on an SGI supercomputer with 64 CPUs. The convergence is controlled by mean of mass imbalance, which is defined as the difference between the mass flow rate into the computational domain and that out of the domain, i.e. $(\dot{m}_{in}-\dot{m}_{out})/\dot{m}_{in}$. The mass imbalance goal in the present computations is set to 0.001.

Non-reacting flow

In this subsection, the turbulent mixing (chemical reaction is not considered) of supersonic airflow and hydrogen flow is investigated and used to validate the current code.

Flow structures near the delta-shape strut can be observed in Fig.3, where contour lines of pressure are given. Compared with the shadow-picture (Fig.4) from Overmann's experimental result, the main flow structures are clearly captured, e.g. the shock waves noted as "shock-I" and "shock-II" in the shadow-picture.

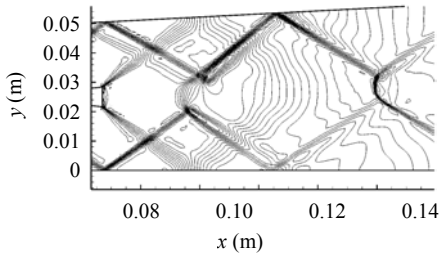

Fig.3 Shock structures near delta-shape strut for the non-reacting case

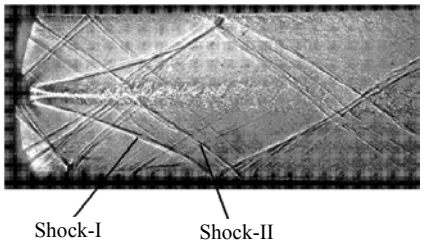

Fig.4 Shadow-picture for the non-reacting case

Fig.5 presents the computed pressure distribution along the upper, lower walls and middle line. Comparison between the computational data and experimental result is given in Fig.6. The discrepancy is obvious in the vicinity of the positions of x=0.13 and x=0.15. The 2D assumption may be a major cause of the discrepancy.

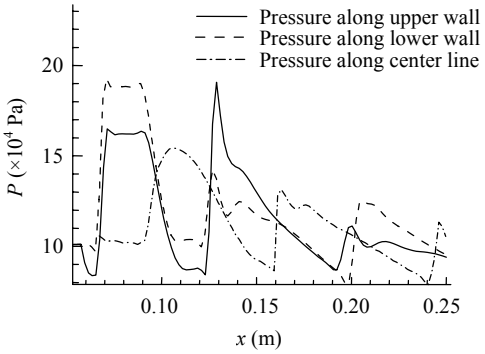

Fig.5 Pressure distributions along walls and the center line for the non-reacting case

Reacting flow

In this subsection the turbulent combustion is investigated. 7 species and 7 reactions are considered

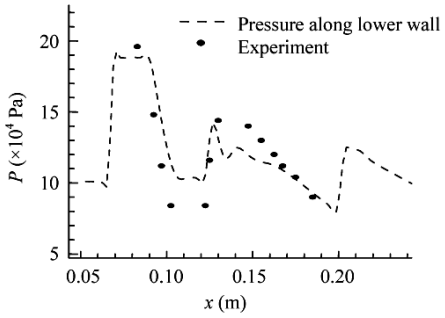

Fig.6 Comparison between the computational data and experimental result for the non-reacting case

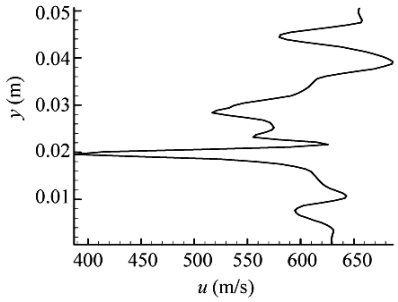

Fig.9 *u*-velocity profiles for the reacting case

in the chemical mechanism (Drummond *et al*., 1991). Comparison between the simulation and the shadow-picture is given in Figs.7 and 8. Turbulent mixing and combustion are obvious in the zone near the combustion flame. The reaction zone of the computational result is broader than that of the experimental picture, especially at the position of x=100 mm.

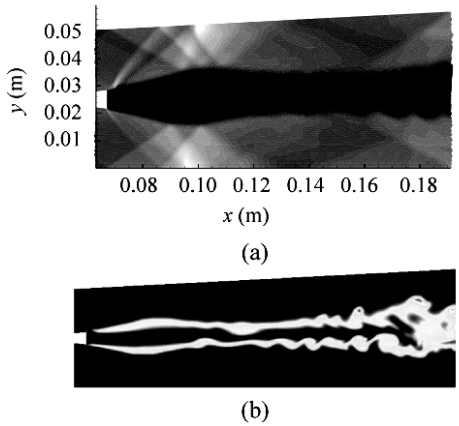

Fig.7 The distribution for the reacting case
(a) Density field; (b) Mass fraction field of H_2O

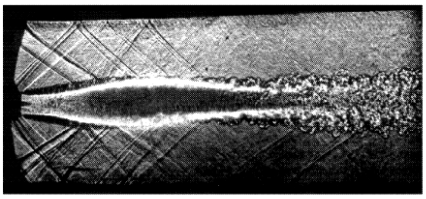

Fig.8 Shadow-picture for the reacting case

Fig.9 shows the instantaneous streamwise velocity profiles calculated at the position of x=78 mm. Complex turbulence can be observed from the velocity profiles. Detailed turbulence data will be achieved and published in the near future.

DISCUSSIONS AND FUTURE WORK

Shih and Liu (2004; 2005)'s PRNS scheme is implemented to model the turbulent combustion in the DLR Scramjet engine. Some qualitative and quantitative results are presented and comparisons with experimental data are given.

In the near future, further work is to be done within this research project:

(1) "Resolution control parameter" R_{cp} is adjusted further to meet the requirement of turbulent combustion simulation.

(2) Finer grids should be created to consider the small turbulence scales. Especially fine elements should be placed in the boundary layer near the walls, and viscous no-slip condition should be used. Then turbulence effect in the boundary layer can be appropriately considered.

(3) True 3D calculation will be conducted to obtain more physical results.

References

Bush, R.H., Mani, M., 2001. A Two-equation Large Eddy Stress Model for High Subgrid Shear. AIAA Paper, No. 2001-2561.

Cai, X.D., Ladeinde, F., 2006. An Evaluation of the Partially-resolved Numerical Simulation Procedure for Near-wall Turbulence Prediction. AIAA Paper, No. 2006-115.

Drummond, J.P., Carpenter, M.H., Riggins, D.W., 1991. Mixing and Mixing Enhancement in Supersonic Reacting Flowfields. *In*: Murthy, S.N.B., Curran, E.T. (Eds.), Progress in Astronautics and Aeronautics Series: High-Speed Flight Propulsion Systems, **137**:383-455,

Fan, T.C., Tian, M., Edwards, J.R., Hassan, H.A., Baurle, R.A., 2001. Validation of a Hybrid Reynolds Averaged/Large Eddy Simulation Method for Simulating Cavity Flameholder Configuration. AIAA Paper, No.

2001-2929.

Georgiadis, N.J., Iwan, J., Alexander, D., Reshotko, E., 2001. Development of a Hybrid RANS/LES Method for Compressible Mixing Layer Simulations. AIAA Paper, No. 2001-0289.

Menter, F.R., Kuntz, M., Bender, R., 2003. A Scale-adaptive Simulation Model for Turbulent Flow Predictions. AIAA Paper, No. 2003-0767.

Nichols, R.H., Nelson, C.C., 2001. Weapons Bay Acoustic Predictions Using a Multiscale Turbulence Model. Proceedings of the 2001 Aircraft Store Compatibility Symposium and Workshop.

Oevermann, M., 2000. Numerical investigation of turbulent hydrogen combustion in a Scramjet using flamelet modeling. *Aerospace Science and Technology*, **4**(7):463-480. [doi:10.1016/S1270-9638(00)01070-1]

Shih, T.H., Liu, N.S., 2004. Partially Resolved Numerical Simulation. AIAA Paper, No. 2004-0160.

Shih, T.H., Liu, N.S., 2005. A Unified Strategy for Numerical Simulation of Turbulent Flows (Private Communication).

Spalart, P.R., Jou, W.H., Strelets, M., Allmaras, S.R., 1997. Comments on the Feasibility of LES for Wings, and on a Hybrid RANS/LES Approach. First AFOSR International Conference on DNS/LES. Ruston, Louisiana, USA, p.137.

Strelets, M., 2001. Detached Eddy Simulation of Massively Separated Flows. AIAA Paper, No. 2001-0879.